AIP | Applied Physics Letters

Defect structure of ultrafine MgB2 nanoparticles

Ali Bateni, Sergej Repp, Ralf Thomann, Selçuk Acar, Emre Erdem, and Mehmet Somer

Citation: Applied Physics Letters **105**, 202605 (2014); doi: 10.1063/1.4902375
View online: http://dx.doi.org/10.1063/1.4902375
View Table of Contents: http://scitation.aip.org/content/aip/journal/apl/105/20?ver=pdfcov
Published by the AIP Publishing

Defect structure of ultrafine MgB_2 nanoparticles

Ali Bateni,[1] Sergej Repp,[2] Ralf Thomann,[3] Selçuk Acar,[4] Emre Erdem,[2,a)] and Mehmet Somer[1,a)]
[1]*Department of Chemistry, Koc University, Rumelifeneri Yolu, Sariyer, Istanbul, Turkey*
[2]*Institut für Physikalische Chemie, Universität Freiburg, Albertstr. 21 79104 Freiburg, Germany*
[3]*Freiburger Materialforschungzentrum (FMF) für Physikalische Chemie, Universität Freiburg, Stefan-Meier Str. 21 79104 Freiburg, Germany*
[4]*Pavezyum Chemicals, Orhanlı Mah. Ulu Sokak, No. 3, 34956 Tuzla, Istanbul, Turkey*

(Received 25 September 2014; accepted 11 November 2014; published online 20 November 2014)

Defect structure of MgB_2 bulk and ultrafine particles, synthesized by solid state reaction route, have been investigated mainly by the aid of X-band electron paramagnetic resonance spectrometer. Two different amorphous Boron (B) precursors were used for the synthesis of MgB_2, namely, boron 95 (purity 95%–97%, $<1.5\,\mu$m) and nanoboron (purity $>98.5\%$, <250 nm), which revealed bulk and nanosized MgB_2, respectively. Scanning and transmission electron microscopy analysis demonstrate uniform and ultrafine morphology for nanosized MgB_2 in comparison with bulk MgB_2. Powder X-ray diffraction data show that the concentration of the by-product MgO is significantly reduced when nanoboron is employed as precursor. It is observed that a significant average particle size reduction for MgB_2 can be achieved only by using B particles of micron or nano size. The origin and the role of defect centers were also investigated and the results proved that at nanoscale MgB_2 material contains Mg vacancies. Such vacancies influence the connectivity and the conductivity properties which are crucial for the superconductivity applications. © *2014 AIP Publishing LLC*. [http://dx.doi.org/10.1063/1.4902375]

Current research interest in nano-sized magnesium diboride (MgB_2) is motivated by novel wire or coil applications such as magnetic resonance imaging (MRI) magnets operating at cryogenic temperatures,[1] engineering applications for electrical power,[2,3] high-speed, high-sensitivity, low voltage sensors,[4] and renewable energy[3,5] due to its relatively high critical transition temperature (T_c) about 39 K.[6] These applications exploit the two band superconducting properties of MgB_2, which results relatively high critical current density (J_c) and critical magnetic field (H_c). The three critical parameters (J_c, H_c, and T_c) have been investigated in detail and reported in a number of comprehensive reviews.[7–9] Despite the interesting studies over last decades, there are still controversy in various properties and particularly the defect structure of undoped MgB_2. It has been emphasized that the disorderness such as defects strongly changes the properties of the MgB_2.[10] Another critical issue is the confinement of the crystallite or particle size to the nano-dimension. Although metal ion or recently popular carbon doping and compound morphology play a decisive role to control materials properties, the synthesis method defines an additional, most crucial role that markedly impacts nature and amount of intrinsic defects and/or impurities.

There are different methods for synthesizing MgB_2 such as high temperature heat treatment,[11] pulse plasma technique,[12] and self-propagating high-temperature synthesis (SHS).[13] One can find more details about the different synthesis techniques of the compound MgB_2 in an outstanding review article.[14] In this work, the defect structure of bulk and nanosized undoped MgB_2 materials and their active role in material properties will be investigated by the aid of electron paramagnetic resonance (EPR) spectroscopy. EPR is well suited for this task since it provides a direct method to monitor different paramagnetic states of vacancies and, thus, complements other experimental techniques such as powder X-ray diffraction (PXRD) and scanning/transmission electron microscopy (SEM/TEM) microscopy. In this sense, EPR does not only work very well on the identification of paramagnetically active intrinsic defects but also one may obtain reliable correlation to the structural and electronic properties of MgB_2. So far, very limited works have been presented for investigating the defect structure by the aid of EPR. Most of the works[15–21] have been dealt with the superconducting critical transition temperature or spin susceptibility at low temperatures. Thus, the defect structure of the pure MgB_2 at room temperature remained unclear. Things become more complicated and controversial when the crystallite size is scaled to the nano-dimension. Such particles have their size and defect related, special characteristics and may show enhanced functionalities.

Both bulk and nanosized MgB_2 samples were prepared by using well-known solid state synthesis techniques. For the bulk and nano specimen, we utilized as starting powders Mg (99.8%) and amorphous boron 95 (B 95 %-97 %), as well as Mg (99.8%) and amorphous nanoboron (B > 98.5%), respectively. All reactant powders were received from the Turkish company Pavezyum Kimya, Istanbul. A typical reaction mixture contained a total of 1 g of Mg and B (molar ratio 1:2) powders which were grinded with a mortar and pestle for 15 min in open air. For both samples, pellets with 13 mm diameter are pressed using hydraulic press by 10 t/cm^2. The pellets were placed into small metal sample holders and then heated in a tube furnace under Ar flow within 1.5 h to

a)Authors to whom correspondence should be addressed. Electronic addresses: emre.erdem@physchem.uni-freiburg.de and msomer@ku.edu.tr.

700 °C, annealed for 2 h and then quenched to room temperature. All products of the heat treatment were analyzed using PXRD method. PXRDs were measured with BRUKER D2 Phaser diffractometer (Cu-Kα_1 radiation (0.1540 nm) with LYNXEYETM detector). The lattice parameters of the two MgB_2 samples were refined using Rietveld method. The quantitative phase analyses of the products were performed employing the TOPAS software. SEM images of powders were taken with Zeiss Ultra Plus FE-SEM at 2 kV accelerating voltage. LEO 912 Omega transmission electron microscopy (TEM) instrument were used with an accelerated voltage of 120 kV. TEM samples were prepared by dispersing the powder in dilute ethanol medium under ultrasonic agitation. A drop of the suspension was placed on a carbon coated one mesh copper grid (EMS CF200-Cu). X-band (9.86 GHz) cw-EPR measurements were performed with Bruker EMX spectrometer. We have used cylindrical super-high-quality (SHQ) resonator from Bruker. The offset in the magnetic field and the exact g-factors in X-band measurements were determined with a polycrystalline DPPH (2-diphenyl-1-picrylhydrazyl) reference sample with well-known g-factor ($g = 2.0036$). The EPR spectral analysis has been performed using the WINEPR program from Bruker.

PXRD patterns of both bulk and nanosized MgB_2 are shown in Fig. 1. In both, MgB_2 and MgO are the final products. Mg deficient borides, such as MgB_4 and MgB_{12}, were not present. Only in bulk MgB_2 a small amount of excess Mg was detected. This can be referred to either not sufficient reaction temperature or too short dwell time of heat treatment for Mg and boron 95 to react. From Rietveld analysis the lattice parameters *a*- and *c*- for nanosized and bulk MgB_2 were calculated as 3.09036(6) Å and 3.5286(1) Å and 3.08856(5) Å and 3.5267(1) Å, respectively. The quantitative Rietveld analysis showed MgB_2 (93.61%), MgO (4.85%), and Mg (1.54%) for bulk and MgB_2 (96.38%) and MgO (3.62%) for nanosized MgB_2. The analysis also reveals that MgO contamination in nanosized MgB_2 is around 1.3% less than in the bulk one. It has been reported that the reduction of MgO strongly increases the connectivity in MgB_2.[22] On the other hand, there are many attempts to remove the EPR inactive MgO from MgB_2 material; however, these methods only reached success for a certain amount of reduction of MgO.[23–25] In our preparation route, it is also not possible to remove MgO completely by annealing.

Figs. 2(a)–2(d) are showing the SEM images of nanoboron, Mg powder, manually grinded Mg with boron 95 and nanoboron powders for 15 min. As depicted in Fig. 2(c), the Mg and B particles are spatially separated from each other. Magnified image of one of the Mg particles clearly reveals that Mg is only partially covered with the boron 95. In contrast, Mg particles grinded with nanoboron are almost completely "coated" (Fig. 2(d)). In addition, mixtures containing nanoboron tend to more agglomeration than those with boron 95. The reason might be the ultrafine size and the higher surface energy of the nanoboron particles, spreading more readily and uniformly over the surface of the Mg particles. Moreover, the wetting ability of nanoboron may reduce the diffusion length and enhance the reaction rate. The result is a complete reaction at considerably lower temperatures. Probably, the unreacted Mg detected in bulk MgB_2 originates from this fact, meaning that 700 °C is not sufficient for a complete reaction of Mg with boron 95.

SEM and TEM images of MgB_2 microstructure synthesized from boron 95 and nanoboron powders are shown in Figs. 3(a)–3(d). In bulk MgB_2, prismatic and well-shaped hexagonal crystals are clearly seen from the SEM images whose particles sizes are in the range of 100–400 nm. Plate like and poor crystallized moieties can be well distinguished in nanosized MgB_2. Low crystallinity might be related to higher amorphous content of the particles with a mean size of 50–250 nm. Furthermore, the Figs. 3(a) and 3(c) reveal that the particles of the nanosized MgB_2 are more uniform and smaller compared to those of bulk MgB_2, as shown in Figs. 3(b) and 3(d). The reason of the different particle sizes in the two MgB_2 samples is closely related to the material properties of the starting B powders. In nanoboron, all particles are <250 nm (50–250 nm) and has a similar particle

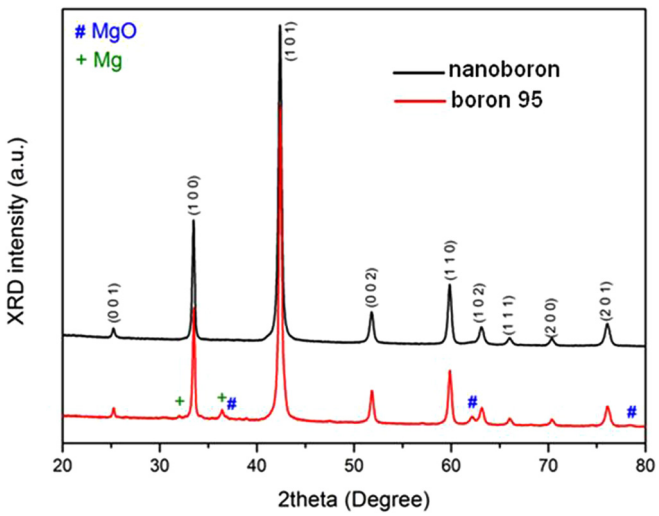

FIG. 1. PXRD patterns of bulk and nanosized MgB_2 synthesized with the reactant powders boron 95 (red) and nanoboron (black), respectively. Diffractions from MgO and Mg in boron 95 (bulk) sample are indicated by the symbols # and +, respectively.

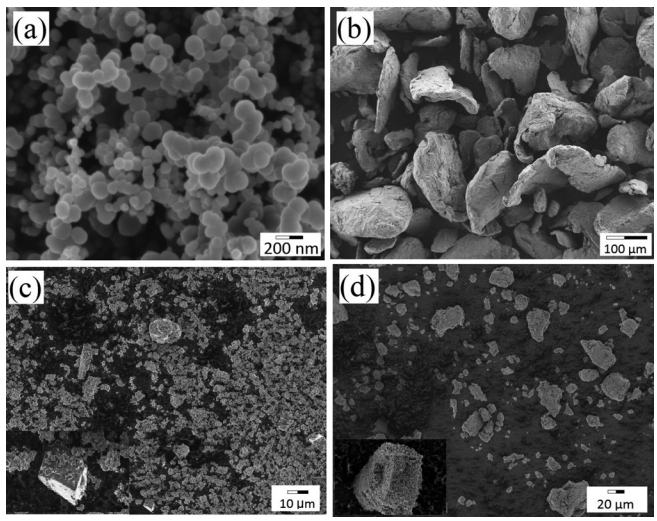

FIG. 2. SEM images of (a) as received nanoboron, (b) as received Mg, (c) manually grinded mixture of boron 95 and Mg, and (d) manually grinded mixture of nanoboron and Mg.

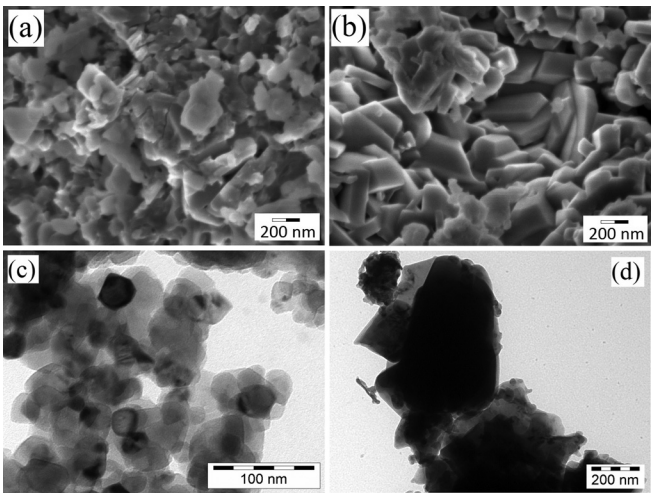

FIG. 3. SEM images of (a) nanosized and (b) bulk MgB_2 powders. TEM images of (c) nanosized MgB_2 and (d) bulk MgB_2 powders. Nanosized and bulk powders were synthesized from nanoboron and boron 95, respectively.

size distribution with the starting B powder, while the size range of boron 95 is quite broad and distributed between 0.05 and 1.5 μm. Most probably, the small crystallites (50–200 nm) observed in Figs. 3(b) and 3(d) which are stemming from the reaction of boron 95 particles of smaller sizes. So far, the role of the particle size of the starting B powders in the quality and performance of bulk MgB_2 has been investigated by several researchers.[26,27] Present results are harmonizing very well with those reported in Refs. 26 and 27, emphasizing the particle size correlation between the B precursor and the final product MgB_2. At this point, two additional points are also worth mentioning and should be underlined: (i) The average particle size of nanosized MgB_2 is similar, even smaller than in the starting nanoboron powder and (ii) the size and morphology of Mg has practically no influence on the MgB_2 particle size.

Fig. 4(a) compares the EPR spectra of the elemental Mg and the MgB_2 obtained from nanoboron samples. This clearly shows that elemental Mg which is used in sample preparation has no paramagnetic impurities thus EPR inactive. The peak-to-peak intensity (I_{pp}) and linewidth (ΔB_{pp}) and the symmetry coefficients A and B were depicted on the EPR spectra in Fig. 4(b). The symmetry ratio A/B gives information about the symmetric behavior of each EPR signal defect centers with respect to particle size. From the definition, the EPR line is supposed to be symmetric when $A/B = 1$, and it is asymmetric when $A/B \neq 1$. In Fig. 4(c), a single EPR line with different lineshapes was observed for bulk and nanosized MgB_2. Both signal at first shows the extreme purity of the material. There are no contaminations or transition metal ion impurities, such as Mn, Fe, Cu, or Co, which can be easily detected by EPR which is extremely sensitive to any kind of paramagnetic metal-ion impurity, with a detection limit of 10^{10} spins.[28] Nanosized MgB_2 reveals totally symmetric feature. On the contrary, the bulk powder signal shows rather asymmetric behavior. This difference can be attributed to the localization of defect centers in nanosized MgB_2 which are delocalized electrons (bound states at the defect site) and defect centers on the bulk which are localized. Possible defect centers in pure MgB_2 material could be the Mg vacancies (V_{Mg}), oxygen vacancies (V_o), boron vacancies (V_B), and the interstitials (O_i or B_i). In particular, influence of Mg vacancy in MgB_2 on structural and superconducting properties has been discussed controversially.[29] According to their g-factors (close to free-electron g factor: 2.0023), given in Fig. 4(c), such defects can be attributed to V_O in bulk MgB_2 sample either on the grain boundaries or on the surface since MgO is present as a secondary phases. On the other hand, dominant contributions from the grains in bulk sample can also increase the asymmetry ratio.[21] That results typical Dysonian lineshape in EPR spectrum, which is given in Fig. 4(c) for the bulk MgB_2. This is characteristic for conductive species[30,31] and strong indication of enhancing the metallic character and influencing the ionic conductivity property due to structural defects, namely, V_O, in bulk MgB_2. The same effect has been reported by the aid of X-ray photoelectron spectroscopy (XPS) and SQUID measurements.[32] In the absence of MgO phase and elemental Mg-excess symmetric line with Lorentzian lineshape were observed for the nanosized MgB_2 implying homogeneous line broadening and also evidencing that the particle size in powder are smaller than the skin depth.[33] The size dependent broadening of linewidth ΔB_{pp} from bulk (5.67 G) to nanosize (13.4 G) can be attributed to the interactions of conduction electrons with phonons associated with V''_{Mg}. The formation of this defect centers can be presented Kröger-Vink notation as

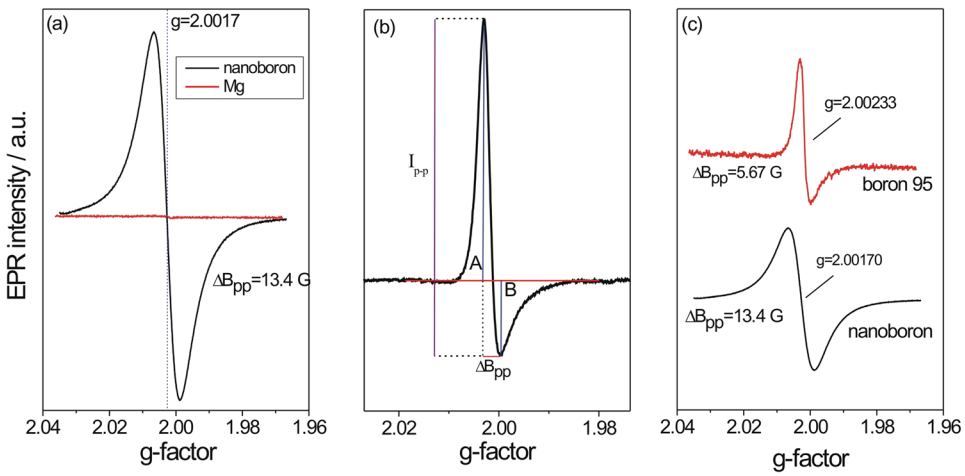

FIG. 4. (a) Comparative EPR spectra of elemental Mg and nanoboron. (b) Definition of symmetry parameter (A/B), peak-to-peak intensity, and the linewidth (ΔB_{pp}) in terms of Dysonian EPR signal. (c) Comparative EPR spectra of MgB_2 obtained from boron 95 and nanoboron.

$$Mg_{Mg}^{\times} + 2B_{B}^{\times} \leftrightarrow 2B' + V''_{Mg}. \quad (1)$$

This is consistent with the inhomogeneously distributed Lorentzian shape of EPR signal which indicates that the unpaired electrons are not isolated at a certain site but rather in an impurity or conduction band probably hopping from one site to another site. Thus, it can be concluded that V_{Mg} dominantly influences the electronic properties of nanosized MgB_2 from nanoboron even it has high purity and crystallinity (cf. XRD and TEM picture in Figs. 1 and 3(c)). It is also expected that the non-metallic character of nanosized MgB_2 could enhance the intergrain connectivity.[34]

Nanosized MgB_2 is synthesized by using nanoboron and Mg without using any mechanical energy deposition such as ball-milling. SEM images showed that particle sizes in nanosized MgB_2 were in the range of nanoboron precursor and TEM picture is confirmed that the particle size is at nanoscale. This is mainly due to the fact that boron has a 3D structure and MgB_2 a layer one (2D). The reaction between Mg and boron starts with the diffusion of Mg into boron particles, because of the 2D character of MgB_2 structure, the growth of MgB_2 crystals are, however, restricted only in two directions which may result in a smaller particle size compared to the precursor nanoboron. These results showed that size of nanoboron is one of the important factors to control the MgB_2 quality. Moreover, nanoboron presented a good wetting ability and enabled to reduce synthesizing temperature and reaction rate. The present study allows also concluding that the choice of B precursors is of prime importance for the functionality of MgB_2 materials which, in turn, is governed by the particle size. Indeed, there is a linear size correlation between the particles of the reactant B powders and the final product MgB_2. This means that a significant average particle size reduction for MgB_2 can be achieved only by using B particles of submicron or nano size. As mentioned above, an interesting detail is that the average particle size in nanoscale MgB_2 is even smaller than in the starting nanoboron powders. The size and shape of the second reactant Mg powder have practically no influence on the MgB_2 particle diameter. From the point of defect structure, the bulk MgB_2 revealed EPR signal related to V_o, whereas EPR of nanosized sample was dominated by V''_{Mg} indicating enhancement of non-metallic conductivity which arise due to the localization of the unpaired electrons. This may give additional functionalities to MgB_2 at nanoscale for the possible use in relevant superconducting technology fields.

This work was financially supported by the *Deutsche Forschungsgemeinschaft* (DFG) Grant No. Er662/1-2 and Koc University graduate program. We gratefully acknowledge the support of Professor Stefan Weber.

[1]S. K. Chen, K. Y. Tan, A. S. Halim, X. Xu, K. S. B. De Silva, W. K. Yeoh, S. X. Dou, A. Kursumovic, and J. L. MacManus-Driscoll, Supercond. Sci. Technol. **26**, 125018 (2013).
[2]H. Fang, P. Gijavanekar, Y. X. Zhou, P. T. Putman, and K. Salama, IEEE Trans. Appl. Supercond. **15**, 3200 (2005).
[3]L. Trevisani, M. Fabbri, and F. Negrini, Cryogenics **47**, 113 (2007).
[4]M. S. A. Hossain, A. Motaman, X. Xu, K. W. See, Ö. Çiçek, H. Ağıl, E. Ertekin, A. Gencer, K. Cheong, M. Maeda, and S. Dou, Mater. Lett. **91**, 356 (2013).
[5]T. Shintomi, T. Asami, G. Suzuki, N. Ota, T. Takao, Y. Makida, T. Hamajima, M. Tsuda, D. Miyagi, M. Kajiwara, and J. Hirose, IEEE Trans. Appl. Supercond. **23**, 5700304 (2013).
[6]J. Nagamatsu, N. Nakagawa, T. Muranaka, Y. Zenitani, and J. Akimitsu, Nature **410**, 63 (2001).
[7]C. Buzea and T. Yamashita, Supercond. Sci. Technol. **14**, R115 (2001).
[8]A. L. Ivanovskii, Phys. Solid State **45**, 1829 (2003).
[9]I. K. Yanson and Y. G. Naidyuk, Low Temp. Phys. **30**, 261 (2004).
[10]T. A. Prikhna, M. Eisterer, H. W. Weber, W. Gawalek, V. V. Kovylaev, M. V. Karpets, T. V. Basyuk, and V. E. Moshchil, Supercond. Sci. Technol. **27**, 044013 (2014).
[11]X. Chen, T. Xia, M. Wang, W. Zhao, and T. Liu, Physica C **454**, 38 (2007).
[12]J. Schmidt, W. Schnelle, Y. Grin, and R. Kniep, Solid State Sci. **5**, 535 (2003).
[13]K. Przybylski, L. Stobierski, J. Chmist, and A. Kołodziejczyk, Physica C **387**, 148 (2003).
[14]J. Karpinski, N. D. Zhigadlo, S. Katrych, R. Puzniak, K. Rogacki, and R. Gonnelli, Physica C **456**, 3 (2007).
[15]M. K. Bhide, R. M. Kadam, M. D. Sastry, A. Singh, S. Sen, D. K. Aswal, S. K. Gupta, and V. C. Sahni, Supercond. Sci. Technol. **14**, 572 (2001).
[16]Y. Köseoglu, B. Aktas, F. Yildiz, D. K. Kim, M. Toprak, and M. Muhammed, Physica C **390**, 197 (2003).
[17]V. Likodimos and M. Pissas, Phys. Rev. B **65**, 172507 (2002).
[18]F. J. Owens, Physica C **363**, 202 (2001).
[19]F. Simon, A. Janossy, T. Feher, F. Muranyi, S. Garaj, L. Forro, C. Petrovic, S. Bud'ko, R. A. Ribeiro, and P. C. Canfield, Phys. Rev. B **72**, 012511 (2005).
[20]F. Simon and F. Muranyi, J. Magn. Res. **173**, 288 (2005).
[21]F. Simon, F. Muranyi, T. Feher, A. Janossy, L. Forro, C. Petrovic, S. L. Bud'ko, and P. C. Canfield, Phys. Rev. B **76**, 024519 (2007).
[22]S. Mizutani, A. Yamamoto, J.-I. Shimoyama, H. Ogino, and K. Kishio, Supercond. Sci. Technol. **27**, 044012 (2014).
[23]C. H. Jiang, H. Hatakeyama, and H. Kumakura, Physica C **423**, 45 (2005).
[24]P. Kovac, M. Kulich, W. Haessler, M. Hermann, T. Melisek, and M. Reissner, Physica C **477**, 20 (2012).
[25]K. L. Tan, K. P. Lim, A. S. Halim, and S. K. Chen, Phys. Status Solidi A **210**, 616 (2013).
[26]S. K. Chen, K. A. Yates, M. G. Blamire, and J. L. MacManus-Driscoll, Supercond. Sci. Technol. **18**, 1473 (2005).
[27]Y. Zhang, C. Lu, S. Zhou, and J. Joo, J. Nanosci. Nanotechnol. **9**, 7402 (2009).
[28]C. I. Rablau, S. D. Setzler, L. E. Halliburton, N. C. Giles, and F. P. Doty, J. Electron. Mater. **27**, 813 (1998).
[29]N. D. Zhigadlo, S. Katrych, J. Karpinski, B. Batlogg, F. Bernardini, S. Massidda, and R. Puzniak, Phys. Rev. B **81**, 054520 (2010).
[30]R. Baraki, P. Zierep, E. Erdem, S. Weber, and T. Granzow, J. Phys. Condens. Matter **26**, 115801 (2014).
[31]F. J. Dyson, Phys. Rev. **98**, 349 (1955).
[32]A. Serquis, R. Schulze, Y. T. Zhu, J. Y. Coulter, D. E. Peterson, N. O. Moreno, P. G. Pagliuso, S. S. Indrakanti, V. F. Nesterenko, and F. M. Mueller, MRS Proceedings **689**, 47 (2002).
[33]F. Beuneu and P. Vajda, Phys. Rev. Lett. **76**, 4544 (1996).
[34]C. C. Wang, C. Wang, R. Zeng, and S. X. Dou, J. Appl. Phys. **108**, 023901 (2010).